



## PAPER

[View Article Online](#)  
[View Journal](#) | [View Issue](#)
Cite this: *Nanoscale*, 2024, **16**, 11138

# Donor–acceptor type triphenylamine-based porous aromatic frameworks (TPA-PAFs) for photosynthesis of benzimidazoles †

 Xinmeng Xu,<sup>a</sup> He Wang,<sup>a</sup> Zhenwei Zhang,<sup>b</sup> Jiali Li,<sup>b</sup> Xiaoming Liu,<sup>b</sup>  Xin Tao \*<sup>a</sup> and Guangshan Zhu<sup>a</sup>

The development of efficient and recyclable photocatalysts for organic synthesis is of great interest. This study presents the synthesis of triphenylamine-based porous aromatic frameworks (TPA-PAFs) in an alternating donor–acceptor (D–A) manner. The light absorption range and the optical band gaps of TPA-PAFs are effectively tuned by changing the electron acceptor units, which further determine their photocatalytic properties. As a result, TPA-PAFs exhibit excellent catalytic performance for the photosynthesis of benzimidazoles in high yields (up to 99%), broad substrate scope (18 examples), and good recyclability (up to 10 cycles). This work provides a feasible approach toward the facile design and synthesis of efficient and stable PAF-based photocatalysts, which further broadens the application of PAFs catalytic materials in photocatalytic organic synthesis.

 Received 24th February 2024,  
 Accepted 7th May 2024

DOI: 10.1039/d4nr00779d

[rsc.li/nanoscale](https://rsc.li/nanoscale)

## Introduction

Visible-light-driven photocatalytic reactions have received widespread attention for their advantages of high efficiency, ease of operation, and mild reaction conditions.<sup>1</sup> Photocatalysts are indispensable to realize the conversion of solar energy into chemicals. Most organic molecules are unable to effectively absorb light at visible wavelengths, while suitable photocatalysts can transport electrons and provide active sites thus effectively achieving catalytic transformations.<sup>2</sup> Recently, various classes of photocatalysts have been developed, including semiconductor materials (g-C<sub>3</sub>N<sub>4</sub>,<sup>3</sup> TiO<sub>2</sub>,<sup>4,5</sup> *etc.*), organometallic complexes (Ru(bpy)<sub>3</sub>Cl<sub>2</sub>, bpy = bipyridine,<sup>6</sup> Ir(ppy)<sub>3</sub>, ppy = 2-phenylpyridine,<sup>7</sup> *etc.*), molecular organic dyes (fluorescein,<sup>8</sup> *etc.*) and polymetallic oxides.<sup>9</sup> However, most of these photocatalysts suffer from inherent problems such as poor stability, low recyclability and reusability, and high cost, resulting in limitations for practical applications. Therefore, the development of low-cost, catalytically efficient, easily separable, and metal-free heterogeneous catalysts is a feasible way to solve this problem.

Porous aromatic frameworks (PAFs) with highly stable skeleton structures, high specific surface areas, easy modification and functionalization have emerged as a promising class of porous organic materials in recent years.<sup>10</sup> Recently, PAFs have been extensively applied in various fields such as gas adsorption and separation,<sup>11–13</sup> catalysis,<sup>14</sup> and trace ion extraction.<sup>15,16</sup> In addition, the higher surface area, extended  $\pi$ -conjugated backbone, and lamellar stacking structure of PAFs provide optimal channels for carrier migration and charge separation.<sup>17</sup> Meanwhile, the ability to tune the photo-energy band gap, redox potential, and light absorption range through careful framework design makes PAFs an ideal platform for visible-light-driven catalytic organic transformations.<sup>18,19</sup> Benzimidazoles and their derivatives have attracted considerable attentions due to their biological activities such as antifungal, anticancer, antiviral, analgesic, anti-tuberculosis and anti-arrhythmic.<sup>20–22</sup> Moreover, benzimidazole compounds can be used as engineering materials and are widely used in flame retardant materials,<sup>23</sup> solar cells,<sup>24</sup> corrosion inhibitors<sup>25</sup> and other industries. In view of their immense application prospects, the synthesis of benzimidazoles and their derivatives is of great importance. Currently, there are several synthetic methods that require harsh reaction conditions such as strong acids and high temperatures relying on condensation reactions between *o*-phenylenediamines and carboxylic acid derived compounds, most of which are not conducive to large-scale production and environmental protection. In contrast, the synthesis of benzimidazoles and their derivatives achieved under visible-light-driven conditions is a green

<sup>a</sup>Key Laboratory of Polyoxometalate and Reticular Material Chemistry of Ministry of Education, College of Chemistry, Northeast Normal University, Changchun 130024, P. R. China. E-mail: taox091@nenu.edu.cn

<sup>b</sup>College of Chemistry, Jilin University, Changchun 130012, P. R. China

† Electronic supplementary information (ESI) available. See DOI: <https://doi.org/10.1039/d4nr00779d>

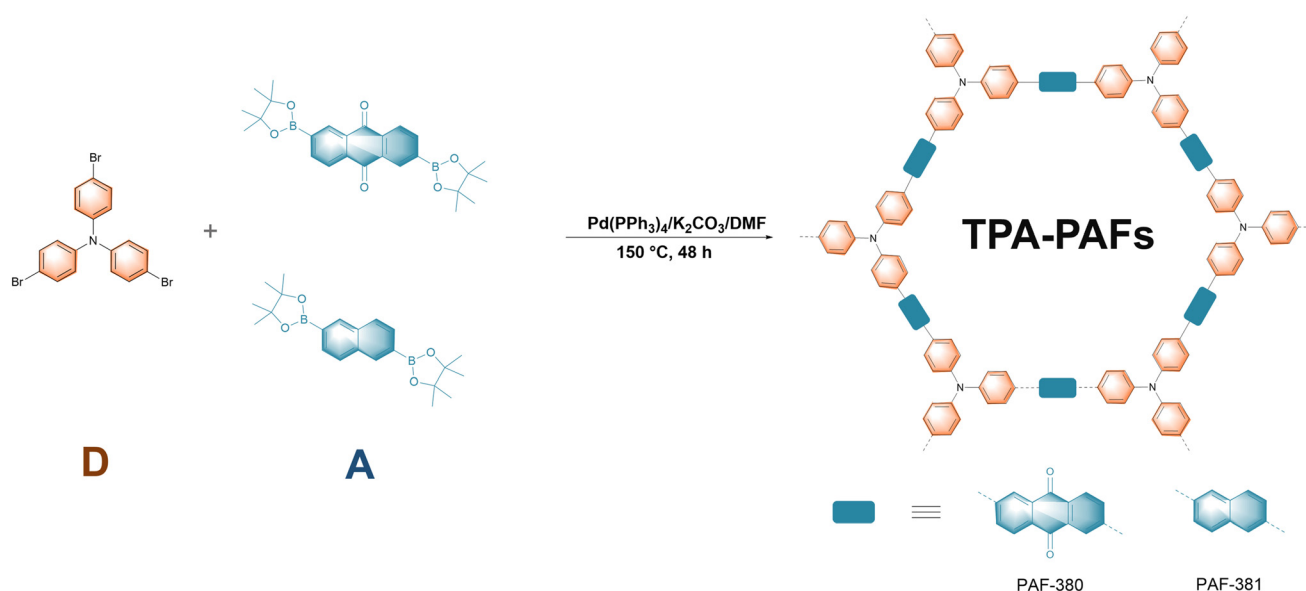
and easy-to-operate synthetic strategy.<sup>26</sup> For example, the Pan group constructed two porous HCPs with the *s*-tetrazine unit, and the suitable energy band structure and pore size enabled efficient photocatalytic synthesis of benzimidazole in ethanol in 99% yield.<sup>27</sup> The Huo group designed and synthesized a novel photocatalyst (BTT-TPA-COF) by a strategy that efficiently regulates the energy band structure and photoelectric properties and achieved the synthesis of benzimidazole in 97% yield.<sup>28</sup> In addition, the Liu group synthesized three CMPs based on benzotrithiophene units and tuned the linking units to precisely regulate the “bandgap engineering”, which realized the efficient photocatalytic synthesis of benzimidazole and its derivatives under an oxygen atmosphere.<sup>29</sup> It is well known that the construction of alternating donor (D)–acceptor (A) type conjugated systems is a very effective method to enhance the separation of photogenerated carriers. By adjusting the structures and ratios of different types of D and A fragments, precise control of the energy band structure and photoelectric properties of D–A type materials can be achieved, which may realize the tailored photocatalysts to meet the requirements for specific catalytic reactions. Therefore, the regulation of energy levels, band gaps and photoelectric properties in PAFs by changing the D–A structure can effectively improve the photocatalytic efficiency.<sup>30,31</sup>

Triphenylamine (TPA) serves as an electron-rich photocatalytic active unit, possessing unique photophysical properties and excellent hole transport. It finds wide applications as a donor in the field of photoelectric chemistry.<sup>32,33</sup> In addition, anthraquinone (AQ) exhibits strong electron-deficient characteristics and unique redox activity,<sup>34</sup> making it suitable as an acceptor in D–A type PAFs. Constructing triphenylamine-based PAFs in combination with different acceptors would be significant for the design and synthesis of organo-

polymeric photocatalysts. Taking these factors into account, two D–A type PAFs containing triphenylamine structural units were synthesized as metal-free heterogeneous photocatalysts (PAF-380 and PAF-381) in this study, and the modulation of the bandgap and energy levels was achieved by varying the connected acceptor units. The incorporation of the D–A system effectively enhances the charge separation, broadens the light absorption range, and reduces the energy bandgap. Under the irradiation of 460 nm blue light, PAF-380 showed excellent catalytic activity for the synthesis of benzimidazoles with good substrate compatibility. Importantly, the structure remains unchanged after ten catalytic cycles with a slight loss of catalytic activity. The energy band analysis and photoelectrochemical experiments reveal the mechanism behind the photocatalytic reaction.

## Results and discussion

As shown in Scheme 1, TPA-PAFs with different electron-acceptor linkers are synthesized in high yields (95% and 91%) *via* palladium-catalysed Suzuki–Miyaura cross-coupling reaction of 2,6-bis(pinacolatoboryl)anthraquinone or 2,6-bis(pinacolatoboryl)naphthalene with tris(4-bromophenyl)amine named as PAF-380 and PAF-381, respectively. The obtained TPA-PAFs are fluffy solid powders that are insoluble in common organic solvents and are stable in dilute acid–base solutions. The TPA-PAFs are characterized by Fourier transform infrared (FT-IR) spectroscopy. The FT-IR spectra of the synthesized TPA-PAFs in comparison with the corresponding monomers are depicted in Fig. 1a and Fig. S1.† The stretching vibration of the aliphatic C–H bonds (2973 cm<sup>−1</sup> and 2992 cm<sup>−1</sup>) of the boronic ester groups in the monomers almost disappeared in PAF-380 and PAF-381, which indicate that the polymerization



**Scheme 1** Syntheses of PAF-380 and PAF-381.

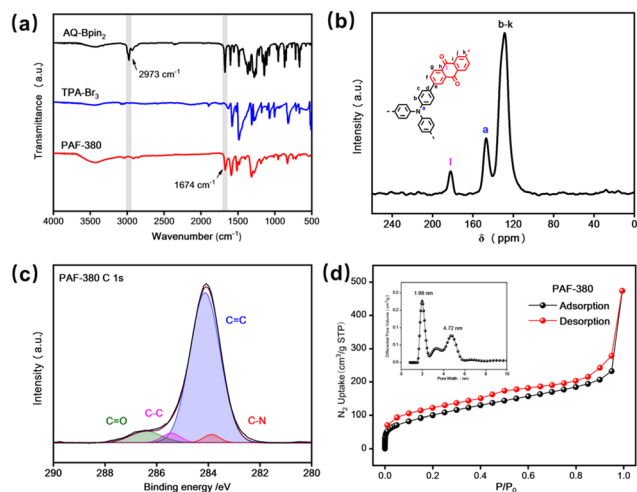


**Fig. 1** (a) FTIR spectra of PAF-380 and starting materials. (b) The solid-state  $^{13}\text{C}$  CP/MAS NMR spectrum of PAF-380. (c) XPS C 1s spectrum of PAF-380. (d) Nitrogen adsorption–desorption isotherm at 77 K and the corresponding pore size distribution profile.

reactions are successful (Fig. 1a and Fig. S1†). Meanwhile, a typical signal of the C=O group in the anthraquinone moiety is observed at  $1674\text{ cm}^{-1}$  in PAF-380. The peak at  $1596\text{ cm}^{-1}$  in the PAF-381 could be attributed to the stretching vibration of the aryl ring skeleton. These results indicate that the anthraquinone and naphthalene structural units are successfully introduced into the conjugated skeleton of PAF-380 and PAF-381. The characteristic signals observed for PAF-380 are consistent with PTPA-AQ reported by Samanta *et al.*<sup>35</sup> The solid-state  $^{13}\text{C}$  cross-polarized magic angle spinning (CP/MAS) nuclear magnetic resonance shows the signals at 146 ppm for aromatic carbon attached to the nitrogen atom in both TPA-PAFs (Fig. 1b). The signal at 182 ppm in PAF-380 could be assigned to the carbonyl group in the anthraquinone unit. The aromatic carbon atoms of PAF-381 are located at 113–142 ppm (Fig. S2†). These results suggest that the TPA-PAFs are successfully synthesized. The elemental composition and chemical bonding of the synthesized TPA-PAFs are also characterized by X-ray photoelectron spectroscopy (XPS). In the C 1s XPS spectrum of PAF-380, four peaks with binding energies of 284.85, 284.11, and 285.42 eV are attributed to C–N, C=C, and C–C, respectively. In addition, the characteristic signal of C=O at 286.42 eV (Fig. 1c) is observed as well. The single peak at 399.92 eV in N 1s XPS spectra of PAF-380 indicates that all nitrogen atoms exist in the form of C–N bond (Fig. S3b†). The characteristic signal of C=O at 531.34 eV and a peak at 532.68 eV also appeared in O 1s XPS spectrum of PAF-380 (Fig. S3c†), which may be caused by the adsorption of oxygen and water from the surface of PAF-380.<sup>36,37</sup> The nitrogen adsorption isotherms of the two TPA-PAFs are measured at 77 K (0–1 bar) (Fig. 1d). The Brunauer–Emmett–Teller (BET) surface area of PAF-380 and PAF-381 are  $356\text{ m}^2\text{ g}^{-1}$ , and  $189\text{ m}^2\text{ g}^{-1}$ , respectively. The PAF-380 pore size distribution calculated using the nonlocal density-functional theory (NL-DFT) model is at

1.9 nm and 4.8 nm, and the PAF-381 pore size distribution is mainly concentrated at 1.9 nm. In contrast, PAF-380 with a higher surface area and abundant mesopores could provide suitable transport channels for the reactants and the products in the photocatalytic process. The powder X-ray diffraction (PXRD) curves indicate that PAF-380 and PAF-381 are amorphous (Fig. S5†). Thermogravimetric analysis (TGA) under a nitrogen atmosphere shows less than 5% mass loss before  $300\text{ }^\circ\text{C}$  for TPA-PAFs (Fig. S6†). The skeleton starts to collapse with increasing temperature; both TPA-PAFs still maintain 80% of their mass at  $670\text{ }^\circ\text{C}$ , indicating their excellent thermal stability. The scanning electron microscopy (SEM) images showed a micrometre-scale morphological structure for TPA-PAFs. PAF-380 shows an irregular morphology and PAF-381 shows an aggregated spherical particle morphology (Fig. 2a and b). The high-resolution transmission electron microscopy (TEM) images show that PAF-380 does not have a long-range ordered crystalline structure, which is consistent with the PXRD results (Fig. 2c). The elemental mapping of energy dispersive X-ray spectra collected in the TEM analyses clearly showed that C, N and O elements are uniformly distributed on the skeleton of PAF-380 (Fig. 2d–f).

The light absorption range of TPA-PAFs is accurately detected by UV-visible diffuse reflectance spectroscopy (Fig. 3a). A wide range of light absorption by PAF-380, up to about 600 nm, with high intensity in both the UV and visible regions is observed. In contrast, the maximum absorption range of PAF-381 is up to about 450 nm. This also corresponds to the colour difference between PAF-380 (dark red) and PAF-381 (yellow green). The optical band gaps ( $E_g$ ) of the TPA-PAFs calculated based on Tauc plots are 1.94 eV and 2.72 eV, respectively (Fig. 3b). To evaluate the energy levels of the TPA-PAFs, electrochemical Mott–Schottky analysis is performed (Fig. 3c), which reveals that the conduction band (CB) edges of PAF-380 and PAF-381 are  $-0.93\text{ V}$  and  $-1.17\text{ V}$ , respectively. The valence band (VB) values of PAF-380 and PAF-381 were calculated to be 1.01 eV, and 1.56 eV by combin-

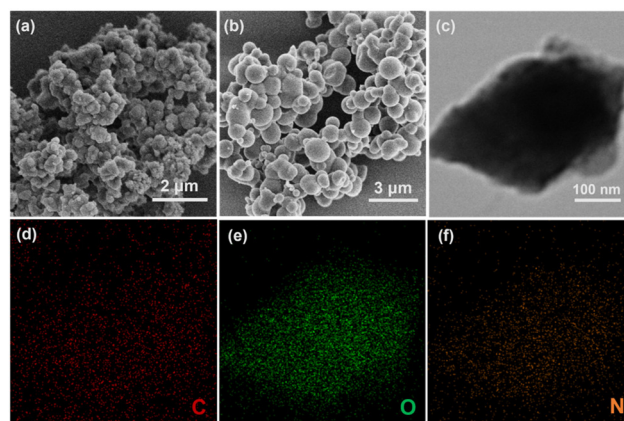


**Fig. 2** SEM images of PAF-380 (a) and PAF-381 (b). (c) TEM image of PAF-380. TEM elemental mapping images of C (d), O (e), and N (f) for PAF-380.

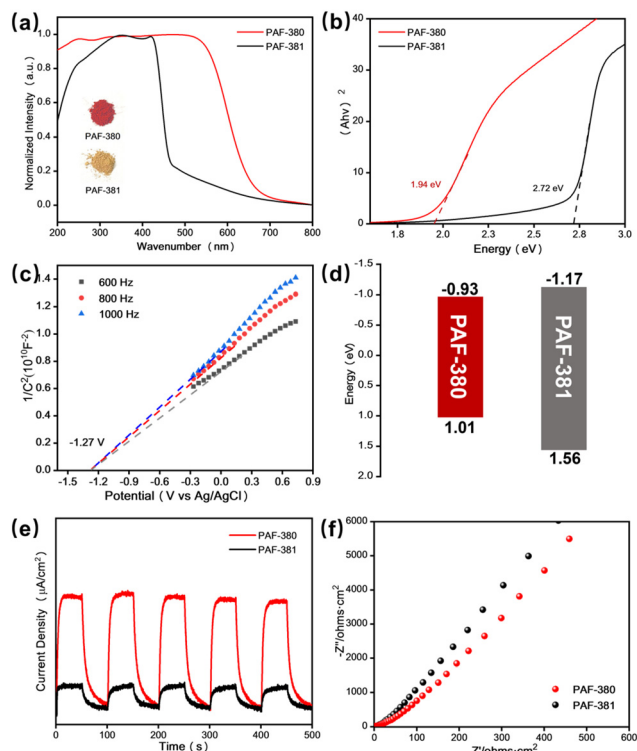


**Fig. 3** (a) Solid-state absorption profiles of TPA-PAFs, insets: the corresponding images. (b) Tauc plots of TPA-PAFs. (c) Mott-Schottky plots of PAF-380. (d) Schematic energy band structure of TPA-PAFs. (e) Transient photocurrent response graph of TPA-PAFs under light irradiation. (f) The Nyquist plots of TPA-PAFs.

ing the optical bandgap and CB values (Fig. 3d). These results indicate that connecting different acceptor units can effectively modulate the energy band structure of TPA-PAFs. It is well known that the separation efficiency and transport rate of photogenerated electrons and holes are crucial for photocatalytic efficiency. Therefore, we further investigate the photoelectric properties of TPA-PAFs by transient photocurrent response testing and electrochemical impedance spectroscopy (EIS) (Fig. 3e and f). Under visible light irradiation, both TPA-PAFs show obvious intermittent on-off irradiation response. PAF-380 exhibits a higher intensity of photocurrent, compared with PAF-381, suggesting that electrons and holes could be separated and transferred rapidly to the surface of the catalyst. In addition, both TPA-PAFs exhibit similar impedances, where PAF-380 has a smaller resistance value than PAF-381. These results imply that the introduction of different acceptors could affect their photogenerated charge separation and transfer efficiency.

The unique features such as excellent stability, porous nature, and a wide range of light absorption of TPA-PAFs make them potential candidates as photocatalysts for the synthesis of organic compounds, such as benzimidazoles and their derivatives. To evaluate the photocatalytic activity of TPA-PAFs, we selected the condensation cyclization reaction between 1,2-phenylenediamine (**1a**) and benzaldehyde (**2a**) as a model reac-

tion to optimize the photocatalytic reaction conditions (Table 1). Under the irradiation of a 460 nm blue LED light (30 W), this reaction proceeds well under an air atmosphere using PAF-380 as the photocatalyst in a protic solvent (e.g. ethanol) giving product **3a** in 94% yield after 2 h (Table 1, entry 1). Under similar conditions, much lower yields ranging from 5% to 23% in aprotic solvents such as *N,N*-dimethylformamide (DMF), tetrahydrofuran (THF), toluene,  $\text{CH}_3\text{CN}$ , acetone and  $\text{CH}_2\text{Cl}_2$  are obtained for the PAF-380 catalysed photosynthesis of compound **3a** (Table 1, entries 2–7). This is probably because ethanol may affect the production of photo-induced electrons and holes, which could further facilitate the electron transfer process and stabilize the reaction products.<sup>38</sup> In contrast, PAF-381 shows lower photocatalytic activities than PAF-380 for this reaction giving compound **3a** in 0–79% yields (Table 1, entries 8–14). This is because the introduction of AQ acceptor to TPA-PAFs could increase its photogenerated charge separation efficiency, which further determines its excellent photocatalytic performance. It is also found that the catalyst dosage is another crucial factor for their photocatalytic performance. It is worth noting that increasing the amount of PAF-380 does not positively affect the catalytic efficiency (Table 1, entries 15–18). The optimal photocatalyst dosage is found to be 2 mg (5.3 mol%). This phenomenon could be attributed to the impeded diffusion caused by the high concentration of the solid catalyst, which results in an unsatisfactory light absorption efficiency.

**Table 1** Optimization of the reaction conditions<sup>a</sup>

Entry	Catalyst	(mg, mol%) <sup>b</sup>	Solvent	Yield <sup>c</sup> (%)
1	PAF-380	2 mg, 5.3 mol%	Ethanol	94%
2	PAF-380	2 mg, 5.3 mol%	DMF	23%
3	PAF-380	2 mg, 5.3 mol%	THF	5%
4	PAF-380	2 mg, 5.3 mol%	Toluene	20%
5	PAF-380	2 mg, 5.3 mol%	$\text{CH}_3\text{CN}$	22%
6	PAF-380	2 mg, 5.3 mol%	Acetone	18%
7	PAF-380	2 mg, 5.3 mol%	$\text{CH}_2\text{Cl}_2$	15%
8	PAF-381	2 mg, 6.8 mol%	Ethanol	79%
9	PAF-381	2 mg, 6.8 mol%	DMF	13%
10	PAF-381	2 mg, 6.8 mol%	THF	Trace
11	PAF-381	2 mg, 6.8 mol%	Toluene	Trace
12	PAF-381	2 mg, 6.8 mol%	$\text{CH}_3\text{CN}$	11%
13	PAF-381	2 mg, 6.8 mol%	Acetone	9%
14	PAF-381	2 mg, 6.8 mol%	$\text{CH}_2\text{Cl}_2$	7%
15	PAF-380	1 mg, 2.6 mol%	Ethanol	87%
16	PAF-380	3 mg, 7.9 mol%	Ethanol	93%
17	PAF-380	4 mg, 10.6 mol%	Ethanol	90%
18	PAF-380	5 mg, 13.2 mol%	Ethanol	89%
19 <sup>d</sup>	PAF-380	2 mg, 5.3 mol%	Ethanol	99%
20 <sup>e</sup>	PAF-380	2 mg, 5.3 mol%	Ethanol	80%

<sup>a</sup> *o*-Phenylenediamine (0.2 mmol), benzaldehyde (0.2 mmol), solvent (3.0 mL), 460 nm blue LED light (30 W, 0.11 W cm<sup>-2</sup>), 298 K, 2 h. <sup>b</sup> The molar ratio of repeating units of the catalysts *versus* substrates. <sup>c</sup> Isolated yields. <sup>d</sup> Reaction time: 3 h. <sup>e</sup> Under irradiation of 460 nm blue LED light (24 W, 0.08 W cm<sup>-2</sup>). rt: room temperature.



Furthermore, the reaction yield is increased by extending the reaction time to 3 h under similar reaction conditions, which resulted in 99% yield (Table 1, entry 19). In addition, photocatalytic experiments under the irradiation of a low wattage 460 nm blue LED lamp (24 W,  $0.08 \text{ W cm}^{-2}$ ) only afford 80% yield (Table 1, entry 20). Based on the above experimental results, 2 mg (5.3 mol%) catalyst dosage, 30 W blue LED light as the light source, 3 h reaction time, under an air atmosphere, at room temperature would be the optimal reaction conditions for the PAF-380 catalysed photosynthesis of benzimidazole and its derivatives.

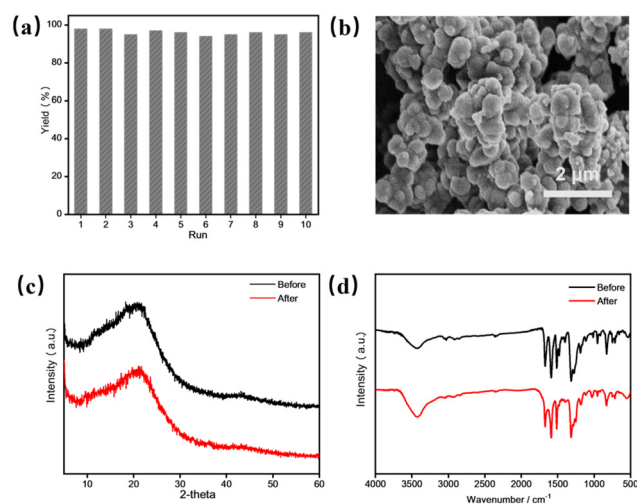
With the optimized reaction conditions in hand, we further explored the compatibility of aldehyde and amine substrates to PAF-380 catalysed photosynthesis of benzimidazole derivatives (Table 2). A series of benzaldehyde derivatives with electron-withdrawing and electron-donating substituents are employed as reaction substrates, which are successfully converted to the

corresponding target products in high yields under the optimized reaction conditions using PAF-380 as the photocatalyst (Table 2, **3b–3j**). For the photosynthesis of the cyano-substituted product **3j**, a longer reaction time (7 h) is required. The yields of the products with electron-withdrawing groups ( $-\text{F}$ ,  $-\text{Cl}$ ,  $-\text{Br}$ ) were found to be higher than those with electron-donating groups ( $-\text{CH}_3$ ). When the same substituent attaches to different positions of the phenyl group of the benzaldehyde, higher yield is found for the *para*-substituted benzaldehydes rather than the *ortho*- and *meta*-substitutions, probably due to the steric hindrance effect. Moreover, a high yield of 90% was achieved using 1-naphthaldehyde as the substrate (Table 2, **3k**). It is noteworthy that PAF-380 also exhibits excellent catalytic performance for aliphatic aldehydes, with yields exceeding 95% for target products **3n** and **3o**. In addition, this catalytic system is equally applicable for heteroatom-containing aromatic aldehydes such as furfuraldehyde or picolinaldehyde, which afford corresponding products (Table 2, **3l–3m**) in yields up to 98%. Furthermore, we also test the suitability of substituted 1,2-benzenediamine substrates (Table 2, **3p–3r**). High yields (94–96%) of substituted benzimidazoles are achieved when 4-chloro or -bromo substituted 1,2-benzenediamine are used as the substrate. A moderate yield (88%) is obtained in the case of 4,5-dimethyl-substituted 1,2-benzenediamine. The above experimental results indicate that PAF-380 shows great substrate compatibility as a photocatalyst for the efficient synthesis of benzimidazole and its derivatives. In parallel, the substrate scope of PAF-381 catalysed photosynthesis of benzimidazole derivatives was also tested (Table S1†), which showed lower yields in comparison with those obtained from the similar conditions under PAF-380 catalysis. Moreover, recyclability is an essential parameter for heterogeneous catalysts. Recycling experiments were conducted to test the recyclability of PAF-380 employing the model reaction of 1,2-benzenedia-

**Table 2** Substrate scope of blue-light-induced condensation cyclization of aldehydes and *o*-phenylenediamines<sup>a,b</sup>

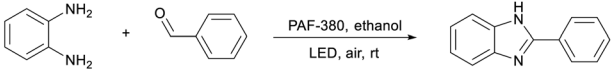
<b>3a</b> (99%)	<b>3b</b> (90%)	<b>3c</b> (92%)
<b>3d</b> (93%)	<b>3e</b> (88%)	<b>3f</b> (91%)
<b>3g</b> (92%)	<b>3h</b> (90%)	<b>3i</b> (95%)
<b>3j</b> (92%) <sup>c</sup>	<b>3k</b> (90%)	<b>3l</b> (98%)
<b>3m</b> (93%)	<b>3n</b> (96%)	<b>3o</b> (97%)
<b>3p</b> (88%)	<b>3q</b> (94%)	<b>3r</b> (96%)

<sup>a</sup> *o*-Phenylenediamine (0.2 mmol), aldehyde (0.2 mmol), PAF-380 (2 mg, 5.3 mol%), ethanol (3.0 mL), air, 3 h, 460 nm blue LED light ( $30 \text{ W}$ ,  $0.11 \text{ W cm}^{-2}$ ), 298 K. <sup>b</sup> Isolated yield. <sup>c</sup> 7 h. rt: room temperature.



**Fig. 4** (a) Reusability of PAF-380 in the photocatalytic synthesis of benzimidazole of **1a** and **2a**. (b) SEM image of PAF-380 after ten cycles. (c) PXRD patterns of PAF-380 before and after ten cycles. (d) FTIR spectra of PAF-380 before and after ten cycles.

**Table 3** Mechanistic study<sup>a,b</sup>

			
Entry	Scavenger	Time (h)	Yield <sup>b</sup> (%)
1	—	2	94%
2 <sup>c</sup>	—	2	25%
3 <sup>d</sup>	—	2	14%
4 <sup>e</sup>	—	2	Trace
5	CuCl <sub>2</sub>	2	34%
6	KI	2	28%
7	BQ	2	72%
8	NaN <sub>3</sub>	2	15%

<sup>a</sup> Reaction conditions: *o*-phenylenediamine (0.2 mmol), benzaldehyde (0.2 mmol), PAF-380 (2 mg, 5.3 mol%), ethanol (3.0 mL), 460 nm blue LED light with 30 W (0.11 W cm<sup>-2</sup>). <sup>b</sup> Isolated yields. <sup>c</sup> In darkness.

<sup>d</sup> Without catalyst. <sup>e</sup> Under N<sub>2</sub> atmosphere. rt: room temperature.

mine with benzaldehyde (Fig. 4a). It is found that PAF-380 can be recycled from the photocatalytic system by simple filtration, washing with ethanol and drying *in vacuo*, and subsequently reused for the next catalytic cycle. After ten cycles there is no obvious loss of photocatalytic activity observed for the PAF-380 catalyst. The recycled PAF-380 material maintains its original aggregation morphology and its chemical structure, indicating that PAF-380 has excellent stability under the conditions applied in the entire photocatalysis and recycling process (Fig. 4b–d). However, the surface area of the recycled PAF-380 decreased (Fig. S9,† SA<sub>BET</sub> = 121 m<sup>2</sup> g<sup>-1</sup>), probably due to the presence of residual organic molecules in its pores. Finally, we explore the applicability of this photocatalytic system for gram-scale synthesis of benzimidazole using 1,2-phenylenediamine and benzaldehyde as reactants (Scheme S1†). A 94% yield (912 mg) of the target product is isolated, indicating that PAF-380 is indeed an efficient and stable photocatalyst that is potentially applicable for large-scale synthesis of benzimidazole and its derivatives.

To gain a mechanistic insight into this photocatalytic reaction system, a series of probe experiments were carried out (Table 3). Lower yields of 25% and 14% are obtained in a dark environment or without the addition of the photocatalyst, respectively (Table 3, entries 2 and 3), indicating that blue light and PAF-380 photocatalyst are both necessary for this catalytic system. There was no production of the target product under a N<sub>2</sub> atmosphere (Table 3, entry 4), demonstrating that oxygen may be essential for the photocatalytic reaction. The reaction yield is obviously inhibited by the addition of CuCl<sub>2</sub> and KI as e<sup>-</sup> scavenger and h<sup>+</sup> scavenger, respectively (Table 3, entries 5 and 6), verifying that electrons and holes are both involved in this photocatalytic reaction process. Furthermore, benzoquinone (BQ) was added to the reaction system as a scavenger of O<sub>2</sub><sup>•-</sup> to verify the reactive oxygen species (Table 3, entry 7), and a slight decrease in yield (72%) is observed. However, an apparent low yield of 15% was obtained when NaN<sub>3</sub> was added to capture <sup>1</sup>O<sub>2</sub> (Table 3, entry 8), indicating

that <sup>1</sup>O<sub>2</sub> plays a dominant role in this photocatalytic reaction system. In addition, 5,5-dimethyl-1-pyrroline-*N*-oxide (DMPO) and 2,2,6,6-tetramethylpiperidine (TEMP) are used as spin trapping agents in the electron spin resonance (ESR) experiments to detect the existence of O<sub>2</sub><sup>•-</sup> and <sup>1</sup>O<sub>2</sub> in PAF-380 photocatalytic system, respectively. As shown in Fig. 5, a typical DMPO-O<sub>2</sub><sup>•-</sup> signal pattern and a typical TEMP-<sup>1</sup>O<sub>2</sub> signal pattern are both observed, which confirms that the two reactive oxygen species O<sub>2</sub><sup>•-</sup> and <sup>1</sup>O<sub>2</sub> are both produced in the PAF-380 photocatalytic synthesis of benzimidazole. It should be noted that a small amount of 2-methylbenzimidazole was detected in the catalytic reaction mixture by gas chromatography-mass spectrometry (GC-MS) (Fig. S10†). This indicates that 2-methylbenzimidazole was formed by the reaction of *o*-phenylenediamine with a small amount of acetaldehyde generated from the oxidation of ethanol.

Based on the above experimental results and the conclusions reported in related literature,<sup>27</sup> a possible reaction mechanism for the photosynthesis of benzimidazoles catalysed by PAF-380 is proposed (Fig. 6). Initially, a condensation

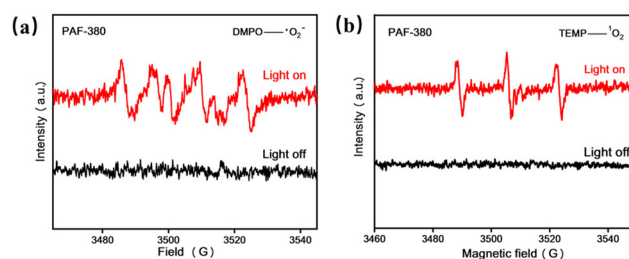


**Fig. 5** (a) ESR spectra of PAF-380 (2.0 mg mL<sup>-1</sup>) and DMPO (0.1 M) in methanol under ambient atmosphere under light irradiation (top) and in darkness (bottom). (b) ESR spectra of PAF-380 (2.0 mg mL<sup>-1</sup>) and TEMP (0.1 M) in methanol under ambient atmosphere under light irradiation (top) and in darkness (bottom).

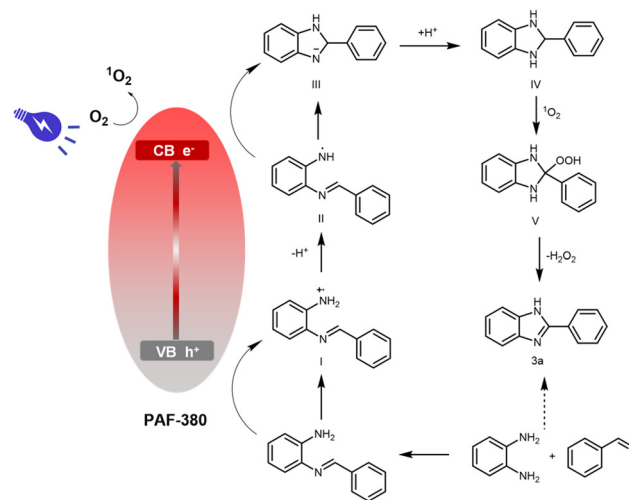


**Fig. 6** Proposed mechanism for the photosynthesis of benzimidazole in the presence of PAF-380 under visible-light irradiation.

reaction between 1,2-benzenediamine and benzaldehyde could occur rapidly to generate 2-(benzylideneamino)aniline. Under the irradiation of blue light, the photogenerated  $h^+$  could oxidize the *in situ* generated 2-(benzylideneamino)aniline to give a nitrogen centered radical cation intermediate **I**, which could be deprotonated to afford a neutral nitrogen centered radical intermediate **II**. Reduction by photogenerated  $e^-$  and ring-closure gives an anionic intermediate **III** that could be easily protonated to generate intermediate **IV**. Oxidation by reactive oxygen species *e.g.*  $O_2^{\cdot-}$  and  $^1O_2$ , and elimination of  $H_2O_2$  (Fig. S11†) finally give target product **3a**.

## Conclusions

In conclusion, two triphenylamine-based D-A type TPA-PAFs have been synthesized from the Suzuki–Miyaura cross-coupling reaction. The surface area, light absorption range and optical band gap were tuned by changing the acceptor units, leading to the enhancement of photocatalytic activity. Compared to PAF-381, the stronger push–pull effect between the electron-donating triphenylamine and more electron-accepting anthraquinone groups in PAF-380 favours the separation of the charge carriers, thus exhibiting excellent catalytic activity for the photosynthesis of benzimidazoles. Moreover, PAF-380 exhibited excellent recyclability, stability, and substrate compatibility. Overall, this work provides a feasible strategy for constructing PAF-based catalytic materials, which further broadens the application of PAF materials in photocatalysis.

## Author contributions

Xinmeng Xu and He Wang: conceptualization, methodology, formal analysis, investigation, resources, data curation, writing – original draft, and writing – reviewing and editing; Zhenwei Zhang and Jiali Li: formal analysis, investigation, resources, and data curation; Xiaoming Liu and Guangshan Zhu: visualization, project administration, and supervision; Xin Tao: validation, resources, writing – original draft, writing – reviewing and editing, visualization, project administration, supervision, and funding acquisition.

## Conflicts of interest

There are no conflicts to declare.

## Acknowledgements

Financial support from the National Natural Science Foundation of China (Grant No. 52173195) is gratefully acknowledged.

## References

- 1 K. Luo, Y. Chen, W. Yang, J. Zhu and L. Wu, *Org. Lett.*, 2016, **18**, 452–455.
- 2 Y. Zhi, S. Ma, H. Xia, Y. Zhang, Z. Shi, Y. Mu and X. Liu, *Appl. Catal., B*, 2019, **244**, 36–44.
- 3 J. Jiang, Z. Xiong, H. Wang, G. Liao, S. Bai, J. Zou, P. Wu, P. Zhang and X. Li, *J. Mater. Sci. Technol.*, 2022, **118**, 15–24.
- 4 Q. Guo, Z. Ma, C. Zhou, Z. Ren and X. Yang, *Chem. Rev.*, 2019, **119**, 11020–11041.
- 5 F. Kayaci, S. Vempati, C. O. Akgun, I. Donmez, N. Biyikli and T. Uyar, *Nanoscale*, 2014, **6**, 5735–5745.
- 6 L. Wang, H. Zhang, Z. Zhang, J. Zhang, Y. He, Q. Li, J. Bao, M. Fang and Y. Wu, *Chem. – Asian J.*, 2023, **18**, e202300297.
- 7 A. K. Clarke, A. P. Parkin, R. J. K. Taylor, W. P. Unsworth and J. A. Rossi-Ashton, *ACS Catal.*, 2020, **10**, 5814–5820.
- 8 Z. Li, H. Song, R. Guo, M. Zuo, C. Hou, S. Sun, X. He, Z. Sun and W. Chu, *Green Chem.*, 2019, **21**, 3602–3605.
- 9 S. Zhao and X. Zhao, *J. Catal.*, 2018, **366**, 98–106.
- 10 Y. Tian and G. Zhu, *Chem. Rev.*, 2020, **120**, 8934–8986.
- 11 P. Zhang, X. Zou, J. Song, Y. Tian, Y. Zhu, G. Yu, Y. Yuan and G. Zhu, *Adv. Mater.*, 2020, **32**, 1907449.
- 12 S. Zhang, J. Li, J. Liu, S. Jiang, X. Chen, H. Ren, T. X. Liu, X. Zou and G. Zhu, *J. Membr. Sci.*, 2021, **632**, 119372.
- 13 W. Wang, Y. Yuan, F. Sun and G. Zhu, *Chin. Chem. Lett.*, 2014, **25**, 1407–1410.
- 14 Y. Yang, Y. Yang, T. Wang, Y. Tian, X. Jing and G. Zhu, *Microporous Mesoporous Mater.*, 2020, **306**, 110393.
- 15 B. Li, Y. Zhang, D. Ma, Z. Shi and S. Ma, *Nat. Commun.*, 2014, **5**, 5537.
- 16 B. Aguila, Q. Sun, H. Cassady, C. W. Abney, B. Li and S. Ma, *ACS Appl. Mater. Interfaces*, 2019, **11**, 30919–30926.
- 17 J. Jiang, R. Luo, X. Zhou, Y. Chen and H. Ji, *Adv. Synth. Catal.*, 2018, **360**, 4402–4411.
- 18 N. Huber and K. A. I. Zhang, *Eur. Polym. J.*, 2020, **140**, 110060.
- 19 J. Wang, P. Zhang, C. Wang, X. Zheng, Y. Zhao, L. Li and S. Miao, *Mater. Des.*, 2020, **186**, 108371–108377.
- 20 S. K. Bagaria, N. Jangir and D. K. Jangid, *Sustainable Chem. Pharm.*, 2023, **31**, 100932.
- 21 K. Chakrabarti, M. Maji and S. Kundu, *Green Chem.*, 2019, **21**, 1999–2004.
- 22 K. Tateyama, K. Wada, H. Miura, S. Hosokawa, R. Abe and M. Inoue, *Catal. Sci. Technol.*, 2016, **6**, 1677–1684.
- 23 T. Liu, Y. Wang, J. Yu and Z. Hu, *Composites, Part A*, 2022, **163**, 107253.
- 24 J. Wang, J. Zhu, C. Li, Y. Lin, Y. Yang, Z. Ma and Y. Lu, *Adv. Funct. Mater.*, 2023, **33**, 2304449.
- 25 J. A. Calderón, F. A. Vásquez and J. A. Carreño, *Mater. Chem. Phys.*, 2017, **185**, 218–226.
- 26 Z. Li, H. Song, R. Guo, M. Zuo, C. Hou, S. Sun, X. He, Z. Sun and W. Chu, *Green Chem.*, 2019, **21**, 3602–3605.
- 27 W.-K. An, S.-J. Zheng, H.-Z. Zhang, T.-T. Shang, H.-R. Wang, X.-J. Xu, Q. Jin, Y. Qin, Y. Ren, S. Jiang, C.-L. Xu, M.-S. Hou and Z. Pan, *Green Chem.*, 2021, **23**, 1292–1299.
- 28 B. Luo, Y. Chen, Y. Zhang and J. Huo, *J. Catal.*, 2021, **402**, 52–60.

- 29 S. Han, Z. Li, Y. Zhi, H. Xia, X. Chen and X. Liu, *J. Mater. Chem. A*, 2021, **9**, 3333–3340.
- 30 S. Ghosh, D. Sarkar, S. Bastia and Y. S. Chaudhary, *Nanoscale*, 2023, **15**, 10939–10974.
- 31 L. Cao, C. Wang, H. Wang, X. Xu, X. Tao, H. Tan and G. Zhu, *Angew. Chem., Int. Ed.*, 2024, e202402095.
- 32 W. Huang, T. Jia, G. Zhou, S. Chen, Q. Hou, S. Luo, G. Shi and B. Xu, *Electrochim. Acta*, 2018, **283**, 1284–1290.
- 33 Y. Wang, G. Ji, W. Ye, F. Zhang, Y. Wang, Y. Zhao and Z. Liu, *ACS Sustainable Chem. Eng.*, 2022, **10**, 9460–9468.
- 34 F. Yu, Z. Zhu, C. Li, W. Li, R. Liang, S. Yu, Z. Xu, F. Song, Q. Ren and Z. Zhang, *Appl. Catal., B*, 2022, **314**, 121467.
- 35 S. Sau and S. K. Samanta, *Chem. Commun.*, 2023, **59**, 635–638.
- 36 C. Dong, J. Chu, L. Cao, F. Cui, S. Liang, X. Zhang, X. Tao, H. Wang and G. Zhu, *CCS Chem.*, 2023, **5**, 607–615.
- 37 X. Dong, Y. Wang, F. Huang and X. Lang, *Chem. Eng. J.*, 2023, **469**, 143934.
- 38 C. Wang and D. Astruc, *Chem. Soc. Rev.*, 2014, **43**, 7188–7216.